Coordinating Distribution System Resources for Co-optimized Participation in Energy and Ancillary Service Transmission System Markets

Chengda Ji, Mohammad Hajiesmaili, Dennice F. Gayme and Enrique Mallada

***Abstract*— This paper investigates the potential of using aggregate controllable loads and energy storage systems from multiple heterogeneous feeders to jointly optimize a utility's energy procurement cost from the real-time market and their revenue from ancillary service markets. Toward this, we formulate an optimization problem that co-optimizes real-time and energy reserve markets based on real-time and ancillary service market prices, along with available solar power, storage and demand data from each of the feeders within a single distribution network. The optimization, which includes all network system constraints, provides real/reactive power and energy storage set-points for each feeder as well as a schedule for the aggregate system's participation in the two types of markets. We evaluate the performance of our algorithm using several trace-driven simulations based on a real-world circuit of a New Jersey utility. The results demonstrate that active participation through controllable loads and storage significantly reduces the utility's net costs, i.e., real-time energy procurement costs minus ancillary market revenues.**

I. INTRODUCTION

Rapidly increasing deployment of distributed energy resources (DERs) (e.g., residential solar panels, electric vehicles (EVs), distributed storage and smart loads) within the distribution network is bringing several new operational challenges to utilities. For example, increased energy production on the distribution side can lead to reverse power flows, as well as both over and under voltages [1]. There is a growing literature investigating these critical operational issues [2]–[14]. However, the disruption of one of the core revenue streams for utilities, the selling of energy to customers, is an equally important, but less studied problem.

To *procure* this energy, utilities participate in day-ahead and real-time electricity markets. In the current market design, the largest portion of energy (roughly 90%) is traded in the day-ahead market based on forecast load and supply for the upcoming (next) day [15]. The real-time market then settles the imbalance between the forecast and actual loads, e.g. 5 minutes ahead of dispatch. Increased penetration of uncertain and intermittent distributed energy resources, reduces the accuracy of day-ahead net load forecasts. This leads to a corresponding rise in the day-ahead market forecast errors and raises the real-time market volume, which can jeopardize utility revenue [16].

A proactive approach for a utility to prevent this type of revenue loss, or to potentially even increase their revenue, is the use of controllable loads and storage systems to strategically procure energy and provide ancillary services within the transmission markets. The utility thus becomes an active real-time market participant; both selling surplus energy procured in the day-ahead market or generated by feeder resources, and using system storage to optimize real-time energy procurement, i.e., arbitrage based on the real-time spot price. Utilities with sufficient resources can also engage in various ancillary service markets, such as spinning or non-spinning reserve markets, and frequency regulation. Toward this, DERs are the critical resources for utilities to participate in such markets. However, there several technical and economic challenges to realizing this potential, which motivates recent interest in studying the potential benefits of using these resources to participate in various energy markets [2]–[11]. For example, [2]–[5] investigate the participation of distributed flexible load resources in the real-time market. The studies in [6], [7] focus on aggregating EV resources to supply energy to the electricity market, while [9]–[11] consider utilizing the aggregate capacity of various types of energy storage systems to participate in real-time energy markets. Ancillary service market participation by DERs has also been considered [2], [8]. Strategic joint participation in real-time and ancillary service markets expands the design space and has the potential to increase utility revenue streams. However, none of these previous works consider the strategic management of DERs for simultaneous participation in both of these markets.

This paper addresses this research gap by designing a distribution network management system that uses aggregate flexible loads and (virtual) storage systems distributed across multiple feeders to co-optimize the participation a utility in the real-time energy and reserve markets. In particular, we formulate a joint optimization problem that simultaneously minimizes the utility's procurement cost in the real-time energy market and maximizes the utility's revenue through participation in the real-time reserve market that dispatches feeder level aggregate DERs connected to the primary distribution feeder. As a first step towards understanding the problem we investigate a deterministic version of this joint-optimization problem, i.e., perfect day-ahead, real-time and ancillary market locational marginal price (LMP) information, and a price-taker scenario such that the price is uniquely determined by the Independent Service Operator (ISO). Key

C. Ji and D. F. Gayme are with Dept. of Mechanical Engineering and E. Mallada is with the Dept. of Electrical and Computer Engineering at the Johns Hopkins University, Baltimore, MD 21218 USA. M. Hajiesmaili is with the College of Information and Computer Sciences at University of Massachusetts Amherst, Amherst, MA 01003. chengdaji@jhu.edu, hajiesmaili@cs.umass.edu, mallada@jhu.edu dennice@jhu.edu Partial support from the U.S. DoE award number DE-EE0008006 (DFG, EM, MH and CJ), and the NSF through grant number EPCN 1711188 (EM and DFG), and CAREER Award number ECCS 1752362 (EM) are gratefully acknowledged.

interactions and potential technical and economic challenges arising from this new operational paradigm are easier to isolate in this simplified setting.

Our formulation takes into account the operational limits and power flow constraints of primary distributions networks and coordinates resources across secondary feeders using an multi-layer aggregate model. More precisely, we consider a radial primary distribution feeder that interconnects multiple transformer banks and coordinates resources across the entire system to participate in different markets; we call this layer the Grid Market Layer (GML). Each bank can have multiple heterogeneous secondary feeders with controllable loads and time-varying energy storage systems. Each each secondary feeder is abstracted as an aggregate controllable generation and virtual storage system that aggregates controllable demands and DERs by performing its own individual optimization, e.g., as proposed in [17]–[19]; we call this layer the Feeder Optimization Layer (FOL). In other words, we assume that the FOL layer is designed to aggregate all of the required information, e.g., solar penetration and real/reactive power charging. The GML objective is to minimize the procurement cost in the real-time energy market and maximize the revenue of obtained in the reserve market. The design space is comprised of the set points of the aggregate generation and charging/discharging patterns of the virtual storage at different feeders, which is provided to each FOL. We use a second-order cone relaxation [20] to transform the GML problem into a second-order cone problem (SOCP), which can be efficently solved using a number of off-the shelf SOCP solvers.

We study the performance of our GML optimization problem by trace-driven experiments using power consumption and generation data traces from two transformer banks, with 4 secondary feeders each, obtained from a local utility in New Jersey (NJ). As excepted, the procurement cost decreases with increasing solar penetration. Our results also confirm that the utility's net costs are decreased through strategic joint participation in the real-time and reserve markets.

The rest of this paper is organized as follows. Section II presents the background and preliminaries related to different electricity markets. Section III is devoted to formulating the GML optimization problem. Numerical simulations are discussed in Section IV. Finally, Section V concludes the paper and outlines directions of ongoing and future work.

II. Preliminaries

In this section we review and discuss the three markets of interest in this work. We then highlight the scenarios under which the utility can profit from such markets.

A. Energy Markets

We consider integrated energy and ancillary service markets that operate in a *two-settlement* procedure that settles transactions at two different timescales and prices, i.e., day-ahead with day-ahead hourly prices, and real-time with spot prices that change every 5 minutes.

1) Day-Ahead Market: In the day-ahead market operation, suppliers and utilities submit their bids for the next day energy and ancillary services, e.g., reserve capacity, selling and buying on an hourly basis. This bidding is based on day-ahead forecasts of generation and demand. After gathering bids from both supply and demand side, the ISO runs a double-auction mechanism and clears the market by determining a day-ahead price.

2) Real-Time Market: In real-time markets, the ISO collects bids from suppliers and utilities and determines the 5-minute real-time spot price based on the actual supply and demand. When the supply is less than the actual demand as compared to the forecast day-ahead demand, the market is up-regulated and the real-time spot price is larger than the day-ahead price, and vice versa. The real-time market operation, thus settles the imbalance between the day-ahead schedule and the real-time actual demand. In this work, we focus on the revenue associated with this imbalance.

3) Ancillary Service Market: There are several types of ancillary services in electricity markets [21]. We can categorize ancillary services into market-based and cost-based services. Market-based services are sold and priced through dynamic markets, similar to energy markets, e.g. operating reserve services. Cost-based services are traded based on their cost which is independent from the market dynamics. Notable examples in this category include reactive supply and voltage control services.

In this work, we focus on market-based ancillary services. More specifically, we focus on the contingency reserves that most ISOs procure both day-ahead and real-time markets. We next describe how the GML interacts with the these markets and the feeders in the distribution system.

B. Market Interaction of the Grid Market Layer

We assume a system in which a utility can control the solar output of a connected set of feeders, and manage the charging/discharging storage systems of each feeder. The GML balances the mismatch between day-ahead and real-time markets using the aggregate flexibility of distributed residential solar panels, and the storage systems for a set of feeders connected to the transmission system at a point of common coupling. The GML optimization further uses the capacity of the feeders to participate in real-time reserve (ancillary service) market. Thus, the GML can sell energy from either surplus generation of the solar generation or discharge of storage to the real-time market when the spot price is high, as well as exploit the virtual storage to participate in real-time reserve markets.

III. The GML Optimization Framework

The goal of GML is to reduce the cost of procuring energy in real-time market by leveraging the aggregate potential of distributed solar generation and small-scale storage systems operating in distribution system feeders. We now develop the GML optimization problem, which coordinates feeder resources across several transformer banks. We assume a time horizon consisting of T equal time slots, each indexed by t.

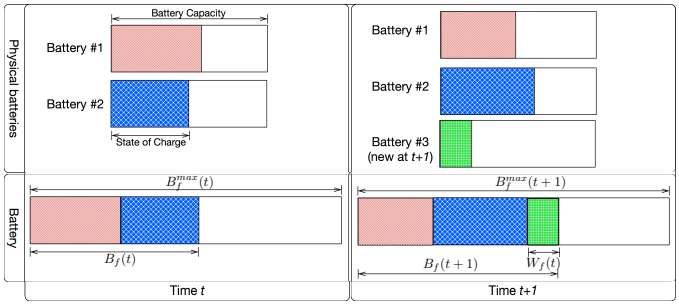

Fig. 1. An illustrative example of the storage model. Each feeder can have several physical storage elements (the upper panels). However, it participates in grid market layer problem by representing a single aggregate storage (the lower panels). The number of physical storage may vary over time. In this example, there are two storage elements at time t for feeder f. At time $t+1$, an additional storage is added to the available physical storage. We define the parameter $W_f(t)$ as the exogenous change in the aggregate storage level to represent this addition (or potentially subtraction) over time.

A. Feeder Level Constraints and Cost Function

We consider a radial primary distribution feeder that interconnects multiple transformer banks. Each bank can have multiple heterogeneous secondary feeders with controllable loads and time-varying energy storage systems. We use $P_f^d(t) \in \mathbb{R}$ and $Q_f^d(t) \in \mathbb{R}$ to denote the real and reactive power (VAr) demands of feeder f at time t. For each feeder we consider two potential sources of real power updates: (i) solar generation (or power response) and (ii) storage.

We use $P_f^g(t) \in \mathbb{R}$ and $Q_f^g(t) \in \mathbb{R}$ to denote the optimization variables associated to the real and reactive power generation of feeder f at time slot t. Each feeder can control its aggregate generation output, within a range of $P_f^g(t) \in [P_f^{\min}(t), P_f^{\max}(t)]$ and $Q_f^g(t) \in [Q_f^{\min}(t), Q_f^{\max}(t)]$, respectively.

The *virtual* storage at each feeder f represents the aggregate energy flexibility within the secondary network, that can be used to participate in market by either charging or discharging. Although the virtual storage usually consists of several physical storage elements or controllable demand, in our model we regard them as a single entity. For examples of market mechanisms available to aggregate storage, we refer the reader to [17]–[19]. We use $B_f(t)$ to denote the storage level at time t.

Then, by letting $B_f^{\min}(t)$ and $B_f^{\max}(t)$ denote the minimum and maximum state of charge of feeder f at time t the storage level is bounded by

$$B_f^{\min}(t) \le B_f(t) \le B_f^{\max}(t).$$

Finally, the evolution of the storage level over time is:

$$B_f(t+1) = B_f(t) - \delta_t R_f(t) + W_f(t),$$

where $W_f(t)$ represents the exogenous change in the storage level of feeder f at t, and $R_f(t) \in \mathbb{R}$ is the optimization variable that denotes the charge/discharge rate of the storage. An illustrative example of our storage model is shown in Fig. 1. Since some of the elements that constitute the aggregate storage may be interfaced to the system using converters, we assume that the virtual storage can deliver or absorb both real and reactive power. Thus VAr injection and absorption rates from the storage at feeder $f \in F$ at time $t \in \mathcal{T}$ are bounded as

$$C_f^{\min}(t) \le C_f(t) \le C_f^{\max}(t), \tag{1}$$

where $C_f(t) > 0$ indicates VAr injection and $C_f(t) < 0$ indicates VAr absorption. This basic formulation can be extended to capture more sophisticated storage models including charging/discharging efficiency and maximum charging/discharging rates using the methods described in [22].

1) Feeder cost function: The cost associated with solar generation $P_f^g(t)$ of feeder f at time t is denoted by $f_{f,t}(P_f^g)$. In general, we consider the cost function to be time varying for each feeder in order to allow it to represent state dependent conditions such as losses, congestion, etc.. Different generation sources might have heterogeneous cost functions. For concreteness, in this paper, we implement a linear function to mimic the cost model of each feeder,

$$f_{f,t}(P_f^g(t)) = \beta_f (P_f^g(t) - P_f^{\max}(t)), \tag{2}$$

where we use the constant β_f to represent the price for solar generation curtailment.[1]

B. Bank Level Constraints

The secondary feeders connect to a primary feeder through transformer banks that ultimately connect to the transmission network. We use a radial primary feeder model with a set of N banks with indexes $i = 1, 2, \cdots, n$, for each bank i, and $\mathcal{T}_i$ denotes the set of (secondary) feeders connected to it. We use $\mathcal{L}$ to denote the set of unordered pairs $\{i, j\}$. Given two banks i and j, $\{i, j\} \in \mathcal{L}$ indicates that the two banks are interconnected by a line with impedance $r_{i,j} + ix_{i,j}$.

We assume transformer banks to be lossless. Therefore the net real and reactive powers flowing through transformer bank i are given by

$$P_i(t) = \sum_{f \in \mathcal{T}_i} \Big(P_f^d(t) - P_f^g(t) - R_f(t) \Big),$$
$$Q_i(t) = \sum_{f \in \mathcal{T}_i} \Big(Q_f^d(t) - Q_f^g(t) - C_f(t) \Big),$$

where P_f^d and Q_f^d are real and reactive power demand at feeder f, P_f^g and Q_f^g are real and reactive solar generation at feeder f, and R_f and C_f are real and reactive power charge/discharge rates of the virtual battery associated with feeder f.

1) Reserve Market Constraints: Most ancillary service markets, and in particular reserve markets, are characterized by three parameters. A response time parameter τ, which specifies the number of real-time slots that the reserve provider has before they are required to be online. A duration parameter k, which specifies the amount of real-time slots that the reserve should be available. And a capacity parameter P_{rsrv}, which represents the amount of reserve scheduled.

[1] A similar cost function can be used to model the marginal change in losses.

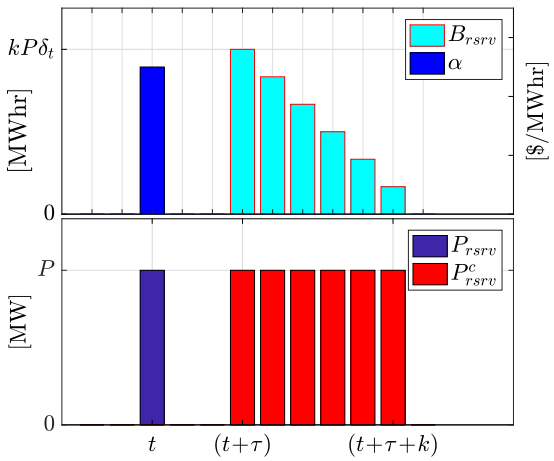

Fig. 2. Evolution of $P_{\mathsf{rsrv}}(t)$, $P^c_{\mathsf{rsrv}}(t)$, and B_{rsrv} given a single ancillary price α at time t. In particular, if the ancillary bid at time t is α, the system instantly reserves $P_{\mathsf{rsrv}}(t) = P$. Then the cumulative reserved power becomes available after τ slots and lasts for k slots $P^c_{\mathsf{rsrv}}(t+\tau+\hat{k}) = P, 0 \le \hat{k} \le (k-1)$. In the meantime, the estimated amount of energy to guarantee a consecutive P^c_{rsrv} at time $t+\tau$ is $B_{\mathsf{rsrv}}(t+\tau) = kP\delta_t$. The future reserved energy is $B_{\mathsf{rsrv}}(t+\tau+\hat{k}) = B_{\mathsf{rsrv}}(t+\tau) - \hat{k}P\delta_t$ with $\hat{k} <= (k-1)$.

For example, in the NYISO, the real-time intervals are 5 minutes, response times are 10 or 30 minutes ($\tau = 2$ and 6) and reserves must be available for 60 minutes ($k = 12$).

We further assume that the utility is allowed to be cleared in consecutive intervals. The cumulative power reserved over the previous τ time steps, i.e. $P^c_{\mathsf{rsrv}}(t)$, is given by

$$P^c_{\mathsf{rsrv}}(t) = \sum_{h=\max\{(t-\tau)-k+1,1\}}^{(t-\tau)} P_{\mathsf{rsrv}}(h). \tag{3}$$

We limit the the total amount of reserves committed at time t as $P^c_{\mathsf{rsrv}}(t) \in [P^{min}_{\mathsf{rsrv}}(t), P^{\max}_{\mathsf{rsrv}}(t)]$.

We provide reserves using storage, which requires an estimate of the minimum amount of energy required to provide a total of $P^c_{\mathsf{rsrv}}(t)$ at time t, which is given by

$$B_{\mathsf{rsrv}}(t) = \delta_t \sum_{l=\max\{(t-\tau)-k+1,1\}}^{(t-\tau)} (l-(t-\tau)+k) P_{\mathsf{rsrv}}(l) \tag{4}$$

where δ_t is the time interval for the real-time market. The virtual batteries available energy must be larger than the energy required for reserves, i.e.,

$$\sum_f B_f(t) \ge B_{\mathsf{rsrv}}(t).$$

Figure 2 illustrates the relationship between $P_{\mathsf{rsrv}}(t)$, $P^c_{\mathsf{rsrv}}(t)$ and B_{rsrv}.

2) Market prices: We use $\lambda^{\mathsf{da}}(t)$ and $\lambda^{\mathsf{rt}}(t)$ to denote day-ahead and real-time market prices at time t. $P^{\mathsf{da}}(t)$ is the day-ahead forecast load, which is an input to the problem. $P_0(t)$ is the actual net demand. As mentioned before, our market cost function is built upon the deterministic market price that is insensitive to changes in $P_0(t)$. This allows us to ignore the price variation caused by inelastic bidding. The electricity market cost can then be represented as

$$P = \sum_{t=1}^{T} \delta_t \left(\lambda^{\mathrm{da}}(t) P^{\mathsf{da}}(t) + \lambda^{\mathrm{rt}}(t) \left(P_0(t) - P^{\mathsf{da}}(t) \right) \right).$$

C. The GML Optimization Problem

We formulate the GML optimization problem as,

$$\begin{aligned} \min \quad & \sum_{t=1}^{T} \delta_t \left(\lambda^{\mathrm{da}}(t) P^{\mathsf{da}}(t) + \lambda^{\mathrm{rt}}(t) \left(P_0(t) - P^{\mathsf{da}}(t) \right) \right) \\ & + \sum_{t=1}^{T} \delta_t \left(\sum_f f_{f,t}(P^g_f(t)) - \alpha(t) P_{\mathsf{rsrv}}(t) \right) \end{aligned}$$

s.t.

Feeder Level:

$$P^{\min}_f(t) \le P^g_f(t) \le P^{\max}_f(t), \tag{5a}$$
$$Q^{\min}_f(t) \le Q^g_f(t) \le Q^{\max}_f(t), \tag{5b}$$
$$B^{\min}_f(t) \le B_f(t) \le B^{\max}_f(t), \tag{5c}$$
$$R^{\min}_f(t) \le R_f(t) \le R^{\max}_f(t), \tag{5d}$$
$$C^{\min}_f(t) \le C_f(t) \le C^{\max}_f(t), \tag{5e}$$
$$B_f(t+1) = B_f(t) - \delta_t R_f(t) + W_f(t), \tag{5f}$$

Bank Level:

$$B_{\mathsf{rsrv}}(t) = \delta_t \sum_{l=\max\{(t-\tau)-k+1,1\}}^{(t-\tau)} (l-(t-\tau)+k) P_{\mathsf{rsrv}}(l), \tag{5g}$$
$$\sum_f B_f(t) \ge B_{\mathsf{rsrv}}(t), \tag{5h}$$
$$P^{\min}_{\mathsf{rsrv}}(t) \le P^c_{\mathsf{rsrv}}(t) \le P^{\max}_{\mathsf{rsrv}}(t), \tag{5i}$$
$$P_i(t) = \sum_{f \in \mathcal{T}_i} \Big(P^d_f(t) - P^g_f(t) - R_f(t) \Big), \tag{5j}$$
$$Q_i(t) = \sum_{f \in \mathcal{T}_i} \Big(Q^d_f(t) - Q^g_f(t) - C_f(t) \Big), \tag{5k}$$
$$P_i(t)^2 + Q_i(t)^2 \le S^{\max}_i(t)^2, \tag{5l}$$
$$(V^{\min}_i(t))^2 \le v_i(t) \le (V^{\max}_i(t))^2, \tag{5m}$$
$$P_{i,k}(t) = r_{i,k} l_{i,k}(t) + P_k(t) + \sum_{m:k\to m} P_{k,m}(t), \tag{5n}$$
$$Q_{i,k}(t) = x_{i,k} l_{i,k}(t) + Q_k(t) + \sum_{m:k\to m} Q_{k,m}(t), \tag{5o}$$
$$\begin{aligned} v_k(t) - v_i(t) = {} & (r^2_{i,k} + x^2_{i,k}) l_{i,k}(t) \\ & - 2(r_{i,k} P_{i,k}(t) + x_{i,k} Q_{i,k}(t)), \end{aligned} \tag{5p}$$
$$l_{i,k}(t) v_i(t) = P_{i,k}(t)^2 + Q_{i,k}(t)^2, \tag{5q}$$
$$P_0(t) = \sum_{i:0\to i} P_{0,i}(t), \tag{5r}$$

where

$$P^g_f(t) \in \mathbb{R}, Q^g_f(t) \in \mathbb{R}, R_f(t) \in \mathbb{R}, C_f(t) \in \mathbb{R},$$
$$P_i(t) \in \mathbb{R}, Q_i(t) \in \mathbb{R}, B_f(t), v_i(t) \in \mathbb{R}, l_{i,k}(t) \in \mathbb{R},$$

$$P_{i,k}(t) \in \mathbb{R}, Q_{i,k}(t) \in \mathbb{R}, P_{\text{rsrv}}(t) \in \mathbb{R}, B_{\text{rsrv}}(t) \in \mathbb{R}.$$

Constraints (5n)-(5o) are for each line $\{i,k\} \in \mathcal{L}$ with series impedance $r_{i,k} + \mathbf{j}x_{i,k}$, and $v_i(t) = |V_i(t)|^2$ is the squared voltage magnitude of bank i at t, and $l_{i,k}(t) = I_{i,k}(t)$ is the squared magnitude of the current flow from bank i to bank k on line $\{i,k\}$. $P_{i,k}(t)$ and $Q_{i,k}(t)$ are the branch real and reactive power flow in line $\{i,k\}$, respectively. $\alpha(t)$ is the ancillary energy price data. A schematic of the optimization variables, and how the GML interacts with the feeders and the transmission system markets is depicted in Figure 3.

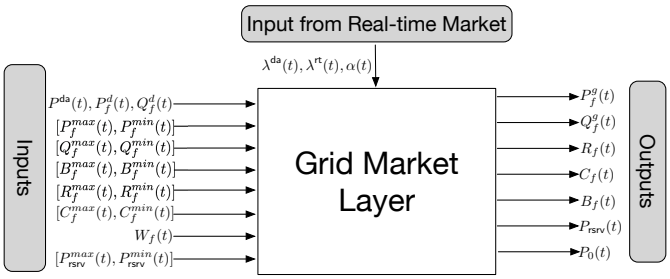

Fig. 3. The inputs and outputs of the GML. As shown the bounds on the solar and storage variables are obtained from the FOL and the prices λ^{da}, λ^{rt}, and α are obtained from the energy and ancillary markets. The GML feeds trajectories of the solar and storage to the FOL and set the ancillary operation trajectory.

To solve this problem we relax the quadratic equalities in (5q) based on the method proposed in [20] to obtain

$$l_{i,k}(t)v_i(t) \geq P_{i,k}(t)^2 + Q_{i,k}(t)^2,$$

which transforms the optimization problem into a second-order cone problem (SOCP). As we consider the connections between feeders and transformer banks to be ideal, i.e., no energy loss, the relaxation is exact, see the condition in [20, Theorem 4].

IV. Simulations

We now provide a set of numerical simulations of a distribution network consisting of two transformer banks, each with 4 feeders representing the a real sub-network of a NJ utility. A schematic of the corresponding 8 feeder circuit is shown in Figure 4. Our simulations use aggregate feeder level time traces for the real and reactive power demand data ($P_f^d(t)$ and $Q_f^d(t)$) as well as the solar generation data ($P_f^{\text{solar}}(t)$) for the circuit obtained from the utility for a day in July 2016. The top panel of Figure 5 summarizes the aggregate power demand and solar generation for all of the simulations.

A. Data Trace Overview and Simulation Setup

In order to simulate a range of solar penetration levels we scale the total available solar power in the following manner

$$P_f^{\max}(t) = \eta_{p.r.} \times P_f^{\text{solar}}(t) \frac{\sum_t P_f^d(t)}{\sum_t P_f^{\text{solar}}(t)}, \tag{6}$$

where $\eta_{p.r.}$ is the penetration level.

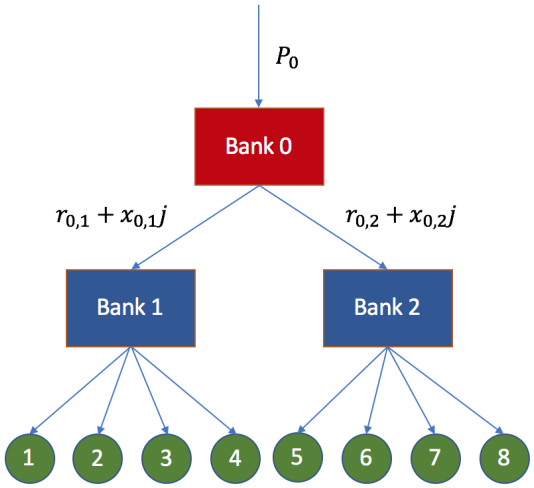

Fig. 4. Schematic of the test system comprised of two transformer banks each with 4 feeders. Bank 0 is connected to the transmission systems. Each transformer bank has an apparent power capability of 35MVA and base voltage at 69kV.

We assume that the storage capacity is 10% of the demand $B_f^{\max}(t) = 10\% P_f^d(t)$. We set the minimum bounds for feeder generation and virtual storage capacity to zero, i.e., $P_f^{\min}(t) = B_f^{\min}(t) = 0$. The reactive power generation bounds are set to $Q_f^{\min}(t) = -0.05 P_f^{\max}(t)$ and $Q_f^{\max}(t) = 0.05 P_f^{\max}(t)$.

We consider exogenous changes $W_f(t)$ in storage availability at feeder f and time t of the form

$$W_f(t) = \begin{cases} 0.1 \times (B_f^{\max}(t+1) - B_f^{\max}(t)), \\ \qquad \text{if } B_f^{\max}(t+1) - B_f^{\max}(t) \geq 0; \\ 0.9 \times (B_f^{\max}(t+1) - B_f^{\max}(t)), \text{ otherwise.} \end{cases}$$

These constraints on exogenous storage changes reflect typical asymmetry expected in the system. For example, an electric vechicle battery added to the system is likely to be empty, whereas one that is removed is likely to be close to fully charged.

We consider both 10 and 30 minute reserve markets, characterized by the response time, respectively $\tau = 2$ and $\tau = 6$, and the commitment duration parameter $k = 12$. The simulations are run for a fixed 24 hour horizon $t \in \{1, \ldots, T = 288\}$, Therefore, is not well defined for $t \in \{1 \ldots \tau\} \cup \{T\}$. To fix this issue, we introduce the following extra constraint

$$B_{\text{rsrv}}(t) = 0, \forall t \in \{[1, \tau] \cup \{T\}\}. \tag{7}$$

The real-time $\lambda^{\text{rt}}(t)$ and ancillary energy price data $\alpha(t)$ are from NYSIO [23].

The day-ahead term $\lambda^{da}(t) P^{\text{da}}(t)$ in the cost function of the optimization problem (5) is constant, since these values are known in advance. Therefore, we can solve the following version of (5) without changing the optimal values of the

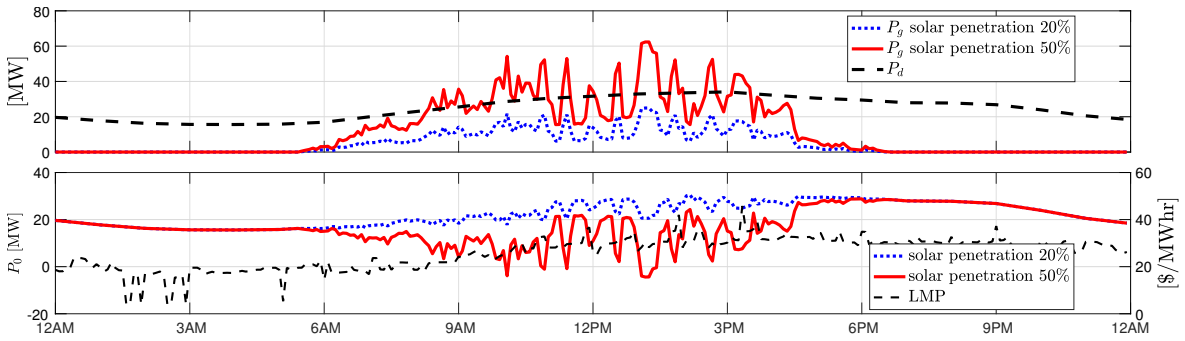

Fig. 5. The top panel shows the total aggregate system demand along with the aggregate solar availability for two penetration levels (20% and 50%). The bottom panel provides the baseline results for a system with solar but no storage or co-optimization of resources.

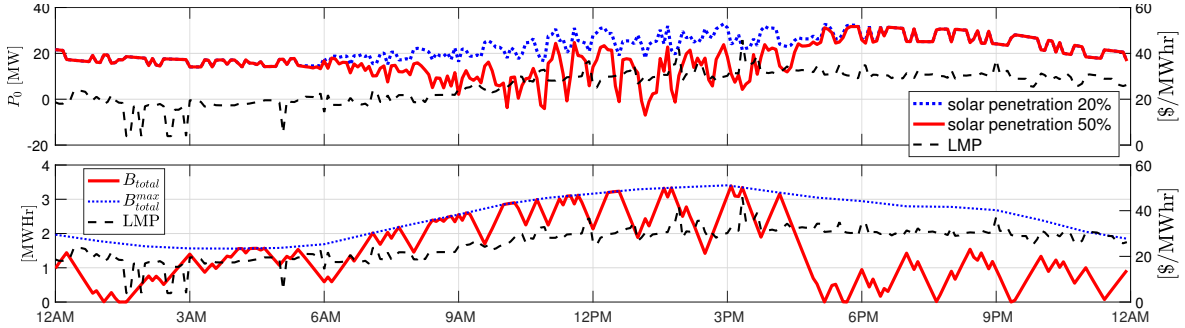

Fig. 6. The top panel indicates the energy procurement $P_0(t)$ without ancillary service market participation (i.e., $\alpha(t) = 0, \forall t$). The lower panel illustrates the storage level and maximum storage capacity for the 20% penetration case along with the LMPs. Here $B_{\text{total}}(t) = \sum_f B_f(t)$, so as the $B^{\max}_{total}(t)$ is the aggregate storage level of the whole network. Only the 20% solar penetration is shown as the dispatch for 50% is essentially the same due to limitations on storage capacity.

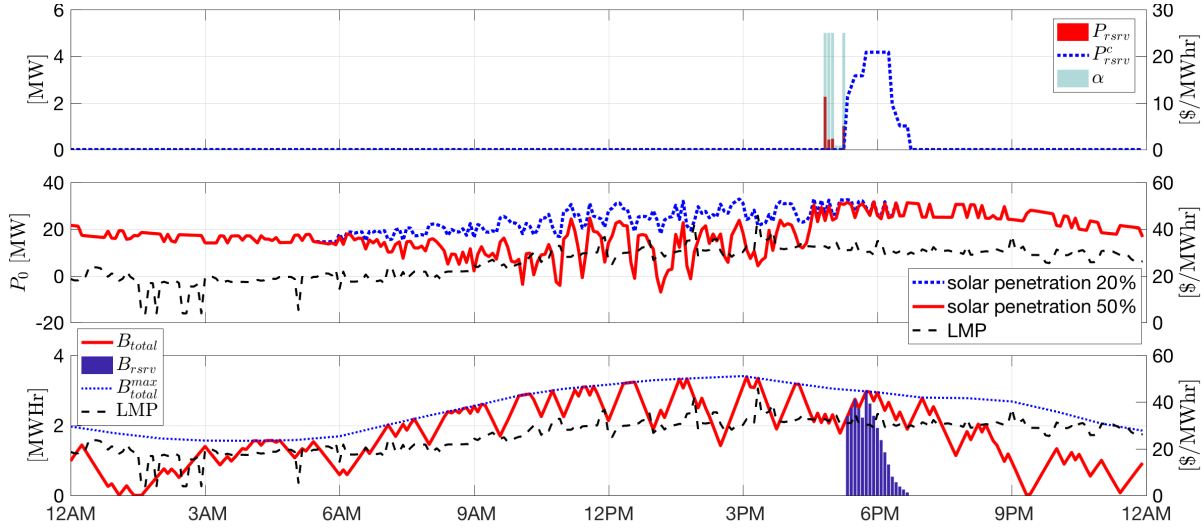

Fig. 7. Simulation for co-optimization of real-time and 30 minute ancillary service markets (with 30 minutes response time and 1 hour participation). The top panel illustrates the scheduled reserve services and the cumulative reserve powers for the 20% penetration case along with the ancillary prices. The center panel shows $P_0(t)$ and the lower panel shows the storage dispatch and use for the reserve market participation for the 20% penetration case

TABLE I

NET RE-BALANCING COST (8).

Scenario	Configuration	Solar 20%	Solar 50%
#1	Baseline (no control)	\$1.76 (0.014%)	-\$8.32 (−0.109%)
#2	Real-time Balancing	-\$77.56 (−0.608%)	-\$87.66 (−1.210%)
#3	Real-time Balancing and 30-min Reserve	-\$82.17 (−0.650%)	-\$92.36 (−1.275%)
#4	Real-time Balancing and 10-min Reserve	-\$265.46 (−2.083%)	-\$275.62 (−3.614%)

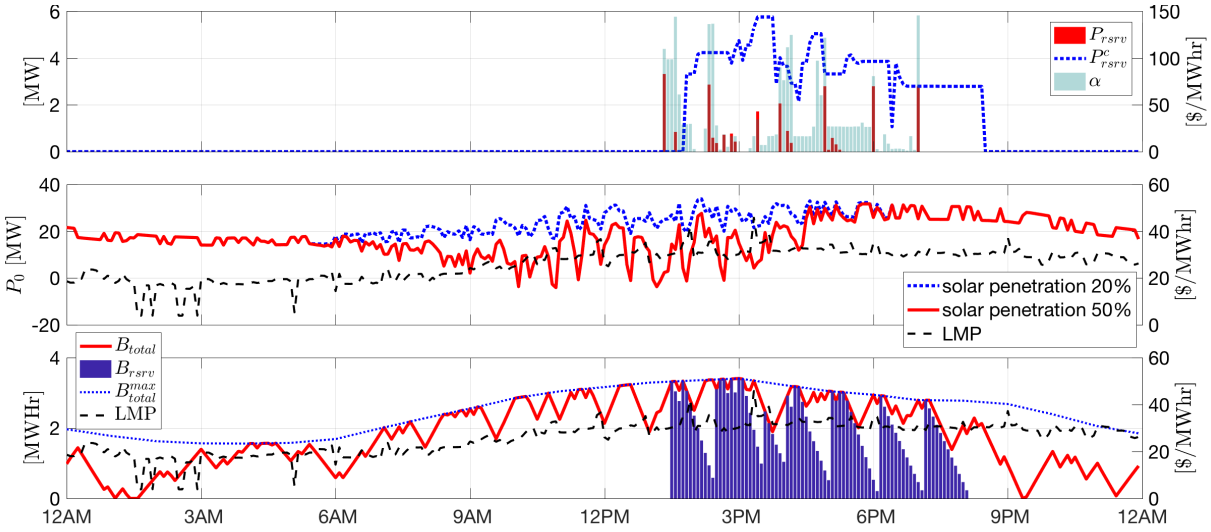

Fig. 8. Simulation for co-optimization of real-time and 10 minute ancillary service markets (i.e. 10 minute respond time and 1 hour participation) with Panel 1 and panel 3 focus on the case with 20% solar penetration.

decision variables.

$$\min \sum_{t=1}^{T} \delta_t \left(\lambda^{\text{rt}}(t)(P_0(t) - P^{\text{da}}(t))\right) + \delta_t \left(\sum_f f_{f,t}(P^g_f(t)) - \alpha(t) P_{\text{rsrv}}(t)\right), \quad (8)$$

$$\text{s.t.} \quad \text{(5a)-(5r)}.$$

The optimal value obtained in (8) represents the net cost of real-time balancing after accounting for reserve participation and feeder cost.

B. Numerical Results

We simulated the following four different instances of the problem, with both 20% and 50% solar penetration.

Scenario #1: This *baseline* scenario assumes battery storage is not available, $B^{max}_f(t) = 0, \forall f, t$, and the solar runs at full capacity, $P^g_f(t) = P^{max}_f(t), \forall t$.

Scenario #2: In the *real-time balancing* scenario we assume that all of the ancillary services prices $\alpha(t) = 0, \forall t$. In other words, the system does not sell capacity to the reserve market and the utility only uses DERs for arbitrage in the real-time market.

Scenario #3: We assume non-zero ancillary service prices for a *30-min reserve market* ($\tau = 6$) with a 60 minutes reserve commitment ($k = 12$).

Scenario #4: The final scenario considers co-optimization between the real-time market and a *10-min reserve market* with 60 a minute reserve commitment (i.e., $\tau = 2$ and $k = 12$). Note that for the particular day considered the average ancillary price for the 10-min market is higher than that of the 30-min market.

Scenarios Cost Comparison: The net balancing costs for all the four scenarios are summarized in Table I. These results show expected trends, i.e., with a higher solar penetration, the optimal cost has a lower value as less energy needs to be procured from the transmission system. When comparing the results vertically (the same scenarios), we can see that when more flexibility is provided to the system, e.g., storage availability, and more profitable options are introduced, e.g, reserves with higher average cost, the net rebalancing cost decreases.

The bottom panel of Figure 5 shows the energy procurement from the transmission system, $P_0(t)$ for the baseline case. Here, the system sells energy to the grid when solar availability exceeds demand. The dispatch associated with cost reductions seen in the second scenario are illustrated in Figure 6, where it is clear that the use of virtual storage allows the system to avoid procuring energy when the LMPs are high. For example, slightly after 3PM, $P_0(t)$ is lower as the system uses storage instead of procuring expensive energy from the transmission system. In general, the storage discharges when the LMPs are high and charge when they

are low (taking advantage of the price differential).

Figure 7 shows the simulation results when the GML co-optimizes the real-time and 30-min reserve market.Similar coordination between high LMP and high solar usage is also seen in this scenario. However, compared with Figure 6, the battery state of charge B_{total} is relatively high when the GML schedules reserves in order to maximize the revenue by reserving some energy in batteries. This only occurs when the reserve revenue is higher than the additional cost incurred through re-balancing.

Figure 8 plots the results from the fourth scenario where the higher average reserve price leads to larger scheduled P^c_{rsrv}, as compared with 30-minute reserve scenario of Figure 7. For example, around 1:30PM and 2PM, the extra reserved capacity requires the system storage to maintain higher energy levels, as shown in panel 3 of Figure 8.

V. Conclusion and Future Work

This work provides a means for a utility to interact with real-time and ancillary markets through a novel hierarchical coordination scheme for secondary distribution feeders over a radial primary network feeder. Specially, we develop a two-layer hierarchical structure in which feeders aggregate DER flexibility, and design a Grid Market Layer interface that can reduce the cost of energy procurement, while guaranteeing operational constraints, by means of strategic participation in real-time and ancillary service markets. We formulate an optimization problem and run several trace driven scenarios that allow us to quantify the benefits of co-optimizing real-time balancing and reserve scheduling. As excepted, we observe a notable decrease in procurement cost that becomes more significant with higher levels of solar penetration. Strategic participation in both the real-time and ancillary service (10 and 30 minute reserve) markets is also shown to reduce net costs.

The proposed framework can be straightforwardly extended to include both price and resource uncertainty through a receding horizon framework in which FOL estimates of resource availability and prices are updated at each time-step. Other promising directions for future work include modeling load elasticity by introducing demand curves into the optimization objective and analyzing price sensitivity to demand variations.

References

[1] G. De Carne, G. Buticchi, Z. Zou, and M. Liserre, "Reverse power flow control in a st-fed distribution grid," *IEEE Trans. Smart Grid*, vol. 9, no. 4, pp. 3811–3819, 2018.

[2] A. Sadeghi-Mobarakeh, A. Shahsavari, H. Haghighat, and H. Mohsenian-Rad, "Optimal market participation of distributed load resources under distribution network operational limits and renewable generation uncertainties," *IEEE Trans. Smart Grid*, 2018, Early Access, doi:10.1109/TSG.2018.2830751.

[3] H. Mohsenian-Rad, "Optimal demand bidding for time-shiftable loads," *IEEE Trans. Power Syst.*, vol. 30, no. 2, pp. 939–951, 2015.

[4] A. Baringo and L. Baringo, "A stochastic adaptive robust optimization approach for the offering strategy of a virtual power plant," *IEEE Trans. Power Syst.*, vol. 32, no. 5, pp. 3492–3504, 2017.

[5] A. Baringo, L. Baringo, and J. M. Arroyo, "Self scheduling of a virtual power plant in energy and reserve electricity markets: A stochastic adaptive robust optimization approach," in *Proc. of the Power Syst. Computation Conf.*, 2018, pp. 1–7.

[6] S. I. Vagropoulos and A. G. Bakirtzis, "Optimal bidding strategy for electric vehicle aggregators in electricity markets," *IEEE Trans. Power Syst.*, vol. 28, no. 4, pp. 4031–4041, 2013.

[7] J. M. Foster and M. C. Caramanis, "Optimal power market participation of plug-in electric vehicles pooled by distribution feeder," *IEEE Trans. Power Syst.*, vol. 28, no. 3, pp. 2065–2076, 2013.

[8] S. Mathieu, Q. Louveaux, D. Ernst, and B. Cornélusse, "A quantitative analysis of the effect of flexible loads on reserve markets," in *Proc. of the Power Syst. Computation Conf.*, Aug 2014, pp. 1–7.

[9] A. Gabash and P. Li, "Flexible optimal operation of battery storage systems for energy supply networks," *IEEE Trans. Power Syst*, vol. 28, no. 3, pp. 2788–2797, 2013.

[10] L. H. Macedo, J. F. Franco, M. J. Rider, and R. Romero, "Optimal operation of distribution networks considering energy storage devices," *IEEE Trans. Smart Grid*, vol. 6, no. 6, pp. 2825–2836, 2015.

[11] S. W. Alnaser and L. F. Ochoa, "Optimal sizing and control of energy storage in wind power-rich distribution networks," *IEEE Trans. Power Syst.*, vol. 31, no. 3, pp. 2004–2013, 2016.

[12] R. Li, Q. Wu, and S. S. Oren, "Distribution locational marginal pricing for optimal electric vehicle charging management," *IEEE Trans. Power Syst.*, vol. 29, no. 1, pp. 203–211, 2014.

[13] Z. Liu, Q. Wu, S. S. Oren, S. Huang, R. Li, and L. Cheng, "Distribution locational marginal pricing for optimal electric vehicle charging through chance constrained mixed-integer programming," *IEEE Trans. on Smart Grid*, vol. 9, no. 2, pp. 644–654, 2018.

[14] S. Huang, Q. Wu, S. S. Oren, R. Li, and Z. Liu, "Distribution locational marginal pricing through quadratic programming for congestion management in distribution networks," *IEEE Trans. Power Syst.*, vol. 30, no. 4, pp. 2170–2178, 2015.

[15] "NYISO power trends 2018," http://www.nyiso.com/public/webdocs/media_room, 2018.

[16] H. Yi, M. Hajiesmaili, Y. Zhang, M. Chen, and X. Lin, "Impact of uncertainty of distributed renewable generation on deregulated electricity supply chain," *IEEE Trans. Smart Grid*, In press, 2017.

[17] J. Liu, N. Zhang, C. Kang, D. S. Kirschen, and Q. Xia, "Decision-making models for the participants in cloud energy storage," *IEEE Trans. Smart Grid*, vol. 9, no. 6, pp. 5512–5521, Nov 2018.

[18] S. Lee, P. Shenoy, K. Ramamritham, and D. Irwin, "vsolar: Virtualizing community solar and storage for energy sharing," in *Proc. of the* 9^{th} *International Conf. on Future Energy Syst.*, 2018, pp. 178–182.

[19] J. T. Huges, A. D. Domínguez-García, and K. Poolla, "Virtual battery models for load flexibility from commercial buildings," in *Proc. of the* 48^{th} *Hawaii International Conf. on Syst. Sciences*, 2015, pp. 2627–2635.

[20] N. Li, L. Chen, and S. H. Low, "Exact convex relaxation of opf for radial networks using branch flow model," in *IEEE SmartGridComm*, Nov 2012, pp. 7–12.

[21] Z. Zhou, T. Levin, and G. Conzelmann, "Survey of US ancillary services markets," Argonne National Lab.(ANL), Argonne, IL (United States), Tech. Rep., 2016.

[22] A. Castillo and D. F. Gayme, "Grid-scale energy storage applications in renewable energy integration: A survey," *Energy Conversion and Management*, vol. 87, pp. 885–894, 2014.

[23] New York Independent System Operator (NYISO), internet:http://www.nysio.com.